

Deep-Sea Research Part II
Manuscript Draft

Manuscript Number: DSR2-D-15-00109

Title: Importance of deep mixing and silicic acid in regulating phytoplankton biomass and community in the iron-limited Antarctic Polar Front region in summer

Article Type: SI: Eddy-Pump

Abstract: Phytoplankton community structure and their physiological response in the vicinity of the Antarctic Polar Front (APF; 44°S to 53°S, centred at 10°E) were investigated as part of the ANT-XXVIII/3 Eddy-Pump cruise conducted in austral summer 2012. Our results show that under iron-limited ($< 0.3 \mu\text{mol}/\text{m}^3$) conditions, high total chlorophyll-a (TChl-a) concentrations ($> 0.6 \text{ mg}/\text{m}^3$) can be observed at stations with deep mixed layer ($> 60 \text{ m}$) across the APF. In contrast, light was excessive at stations with shallower mixed layer and phytoplankton were producing higher amounts of photoprotective pigments, diadinoxanthin (DD) and diatoxanthin (DT), at the expense of TChl-a, resulting in higher ratios of (DD+DT)/TChl-a. North of the APF, significantly lower silicic acid ($\text{Si}(\text{OH})_4$) concentrations ($< 2 \text{ mmol}/\text{m}^3$) lead to the domination of nanophytoplankton consisting mostly of haptophytes, which produced higher ratios of (DD+DT)/TChl-a under relatively low irradiance conditions. The $\text{Si}(\text{OH})_4$ replete ($> 5 \text{ mmol}/\text{m}^3$) region south of the APF, on the contrary, was dominated by microphytoplankton (diatoms and dinoflagellates) with lower ratios of (DD+DT)/TChl-a, despite having been exposed to higher levels of irradiance. The significant correlation between nanophytoplankton and (DD+DT)/TChl-a indicates that differences in taxon-specific response to light are also influencing TChl-a concentration in the APF during summer. Our results reveal that provided mixing is deep and $\text{Si}(\text{OH})_4$ is replete, TChl-a concentrations higher than $0.6 \text{ mg}/\text{m}^3$ are achievable in the iron-limited APF waters during summer.

1 Importance of deep mixing and silicic acid in regulating
2 phytoplankton biomass and community in the iron-limited
3 Antarctic Polar Front region in summer

4 Wee Cheah^{a,b,*}, Mariana A. Soppa^a, Sonja Wiegmann^a, Sharyn Ossebaar^e, Luis M.
5 Laglera^c, Volker H. Strass^a, Juan Santos-Echeandía^d, Mario Hoppema^a, Dieter
6 Wolf-Gladrow^a, Astrid Bracher^{a,f}

7 ^a*Alfred-Wegener-Institute Helmholtz Centre for Polar and Marine Research, Bremerhaven, Germany*

8 ^b*Research Center for Environmental Changes, Academia Sinica, Taipei, Taiwan*

9 ^c*Departamento de Química, Universidad de las Islas Baleares, Balearic Islands, Spain*

10 ^d*Instituto de Investigaciones Marinas de Vigo, Vigo, Spain*

11 ^e*Royal Netherlands Institute for Sea Research, Texel, The Netherlands*

12 ^f*Institute of Environmental Physics, University of Bremen, Bremen, Germany*

13 **Abstract**

14 Phytoplankton community structure and their physiological response in the vicinity of the
15 Antarctic Polar Front (APF; 44°S to 53°S, centred at 10°E) were investigated as part of the
16 ANT-XXVIII/3 Eddy-Pump cruise conducted in austral summer 2012. Our results show
17 that under iron-limited ($< 0.3 \mu\text{mol m}^{-3}$) conditions, high total chlorophyll-a (TChl-a) con-
18 centrations ($> 0.6 \text{ mg m}^{-3}$) can be observed at stations with deep mixed layer ($> 60 \text{ m}$)
19 across the APF. In contrast, light was excessive at stations with shallower mixed layer and
20 phytoplankton were producing higher amounts of photoprotective pigments, diadinoxan-
21 thin (DD) and diatoxanthin (DT), at the expense of TChl-a, resulting in higher ratios of
22 (DD+DT)/TChl-a. North of the APF, significantly lower silicic acid (Si(OH)_4) concentra-
23 tions ($< 2 \text{ mmol m}^{-3}$) lead to the domination of nanophytoplankton consisting mostly of
24 haptophytes, which produced higher ratios of (DD+DT)/TChl-a under relatively low irra-
25 diance conditions. The Si(OH)_4 replete ($> 5 \text{ mmol m}^{-3}$) region south of the APF, on the
26 contrary, was dominated by microphytoplankton (diatoms and dinoflagellates) with lower
27 ratios of (DD+DT)/TChl-a, despite having been exposed to higher levels of irradiance. The
28 significant correlation between nanophytoplankton and (DD+DT)/TChl-a indicates that
29 differences in taxon-specific response to light are also influencing TChl-a concentration in
30 the APF during summer. Our results reveal that provided mixing is deep and Si(OH)_4 is
31 replete, TChl-a concentrations higher than 0.6 mg m^{-3} are achievable in the iron-limited
32 APF waters during summer.

33 *Keywords:* Phytoplankton, photophysiology, nutrients, Antarctic Polar Front

*Corresponding author

Email address: weecheah@gate.sinica.edu.tw (Wee Cheah)

34 1. Introduction

35 The Southern Ocean is of major importance for climate as it is responsible for about
36 40% of the oceanic uptake of atmospheric carbon dioxide (CO₂; [Khatiwala et al. 2009](#)). The
37 extent of CO₂ fluxes in the Southern Ocean varies greatly with space and time ([Landschützer
38 et al., 2015](#)), due mainly to ocean circulation and biological pump ([Hauck et al., 2013](#);
39 [Morrison et al., 2015](#)). In the region north of the Sub-Antarctic Front (SAF) at around
40 45°S, Sub-Antarctic Mode Water and Antarctic Intermediate Water formed during deep
41 winter convection are carrying surface dissolved and phytoplankton-fixed CO₂ into the ocean
42 interior, which results in a large uptake of atmospheric CO₂ in this region ([Rintoul and Trull,
43 2001](#); [Sabine et al., 2004](#); [Morrison et al., 2015](#)). In contrast, south of 45°S is a region of net
44 CO₂ release to the atmosphere as a result of upwelling of CO₂-enriched waters ([Morrison
45 et al., 2015](#)). Rising CO₂ levels in the atmosphere caused by recent anthropogenic activities
46 have driven more CO₂ uptake in the Southern Ocean, altering the spatial distribution of
47 CO₂ fluxes in the Southern Ocean. In particular, the region between 45°S to 55°S, which
48 used to be a net CO₂ release area is now an area of net CO₂ uptake ([Khatiwala et al., 2013](#)).

49 With nitrate (NO₃) and phosphate (PO₄) concentrations in excess all year round, the
50 Southern Ocean has a great potential for primary production, export of organic material,
51 and uptake of CO₂ from the atmosphere. However, limiting factors such as light, iron,
52 silicic acid (Si(OH)₄), and grazing ([Banse, 1996](#); [Boyd, 2002](#); [Hiscock et al., 2003](#)) hinder
53 the full potential of Southern Ocean's biological pump, creating the largest high nutrient low
54 chlorophyll region ([de Baar et al., 2005](#)). In general, the waters north of the APF have typical
55 characteristic of low dissolved iron (DFe), Si(OH)₄, chlorophyll-a (Chl-a) concentrations, and
56 they are dominated by haptophytes, especially in areas remote from continental influence
57 (e.g. [Banse, 1996](#); [Clementson et al., 2001](#); [Hutchins et al., 2001](#)). Surface waters south
58 of the APF are usually rich in macronutrients (NO₃, PO₄, Si(OH)₄) with a phytoplankton
59 community dominated by diatoms ([Alderkamp et al., 2010](#)). Recently, several studies have
60 shown that even in offshore waters away from continental influence, concentrations of DFe,
61 Si(OH)₄, Chl-a, primary production, and phytoplankton composition can differ within a
62 specific zone in the Southern Ocean (e.g. SAZ) ([Bowie et al., 2011](#); [de Salas et al., 2011](#);
63 [Westwood et al., 2011](#)).

64 The physiological response of phytoplankton to different limiting factors (iron, Si(OH)₄,
65 and light) is highly complex and can be multifaceted, especially under co-limitation con-
66 ditions. In addition to nutrient utilisation, the physiological response of phytoplankton to
67 different limiting factors is also imprinted in the coordination of the light harvesting appa-
68 ratus and can result in community shifts ([Falkowski and La Roche, 1991](#)). For example,
69 under iron-light co-limitation conditions, photosynthesis can be limited by light, but the
70 production of light harvesting protein-complexes (e.g. photosystem II and photosystem I)
71 is constrained by iron availability ([Sunda and Huntsman, 1997](#)). In contrast, under low
72 iron high light conditions, photoinhibition or photodamage may occur as iron limitation
73 decreases the synthesis of cytochrome *b₆f* complexes, an enzyme required in the activa-
74 tion of photoprotective mechanisms ([Strzepek and Harrison, 2004](#); [van de Poll et al., 2009](#)).
75 Thus, iron-limited cells are less efficient at coping with an environment with rapid irradiance

76 fluctuations than iron-replete cells (Strzepek and Harrison, 2004; van de Poll et al., 2009;
77 Alderkamp et al., 2012). In addition, under iron-Si(OH)₄ co-limitation conditions, growth
78 of non-silicious, iron-efficient phytoplankton species such as eukaryotic picoplankton and
79 cyanobacteria often dominate over larger cells (Hutchins et al., 2001). This study aims to
80 delineate the respective physiological responses of natural phytoplankton communities un-
81 der varying nutrient and light regimes within a region subjected to CO₂ fluctuation between
82 45°S to 55°S along a meridional transect at 10°E in the Atlantic sector of the Southern
83 Ocean. In particular, photophysiology of phytoplankton under iron-limitation, varying light
84 and macronutrient concentrations conditions north and south of the APF is examined.

85 2. Material and Methods

86 2.1. Study sites

87 Sampling was carried out as part of the “Eddy Pump - ANT-XXVIII/3” cruise along
88 a southbound (43°S-53°S) transect centred at 10°E on board *RV Polarstern* from 11-22
89 January 2012 (Fig. 1). Composite images of Ocean Colour-Climate Change Initiative (OC-
90 CCI) 4-km Chl-a (OC-CCI 2015, <http://www.oceancolour.org>) show that Chl-a was in
91 a declining stage (Fig. 1C-D). Profiles of temperature, salinity and pressure were obtained
92 with a Seabird SBE 911plus CTD (conductivity-temperature-density) mounted on a multi-
93 bottle water sampler. Seawater for phytoplankton pigment, absorption, nitrate+nitrite
94 (NO₃+NO₂), PO₄, and Si(OH)₄ analyses was sampled from Niskin bottles attached to the
95 CTD. Seawater for dissolved iron was sampled using trace-metal clean Go-Flow bottles,
96 independently from the CTD casts.

97 2.2. Mixed layer depth, euphotic depth, and irradiance in the mixed layer

98 The mixed layer depth (z_{ML}) was defined as the first depth at which the density was 0.02
99 kg m⁻³ higher than the surface value (Strass et al., this issue). The euphotic depth (z_{eu})
100 was defined as the depth where downwelling photosynthetically active radiation (PAR) was
101 reduced to 1% of its surface value. z_{eu} was calculated based on the PAR profiles obtained
102 during the optical cast (Section 2.5). Prior to the calculation of z_{eu} , in situ PAR profiles
103 were corrected for variations in solar input based on simultaneously obtained above-surface
104 downwelling irradiance at 490 nm (E_d490) (Smith et al., 1984). E_d490 was measured at 1-
105 min intervals with a RAMSES ACC-VIS hyperspectral radiometer (TriOS GmbH, Germany)
106 located on the uppermost deck of the ship. As surface waves can strongly affect surface PAR
107 measurements, surface PAR at 0 m was extrapolated based on vertical light attenuation
108 coefficient (k_d) between 5 to 21 m following the method of Stramski et al. (2008).

109 For stations without in situ PAR profiles, z_{eu} was calculated from vertical chlorophyll
110 profiles measured with a fluorometer attached the CTD rosette according to the method
111 of Morel and Maritorea (2001). Prior to the calculation of z_{eu} , chlorophyll profiles were
112 smoothed by applying a moving median filter (Strass, 1990). Chlorophyll profiles were
113 linearly regressed with collocated high performance liquid chromatography (HPLC)-derived
114 total Chl-a (TChl-a). HPLC-derived TChl-a was calculated based on the sum of monovinyl
115 Chl-a and chlorophyllide a. Divinyl Chl-a was not detected in our samples. Total daily

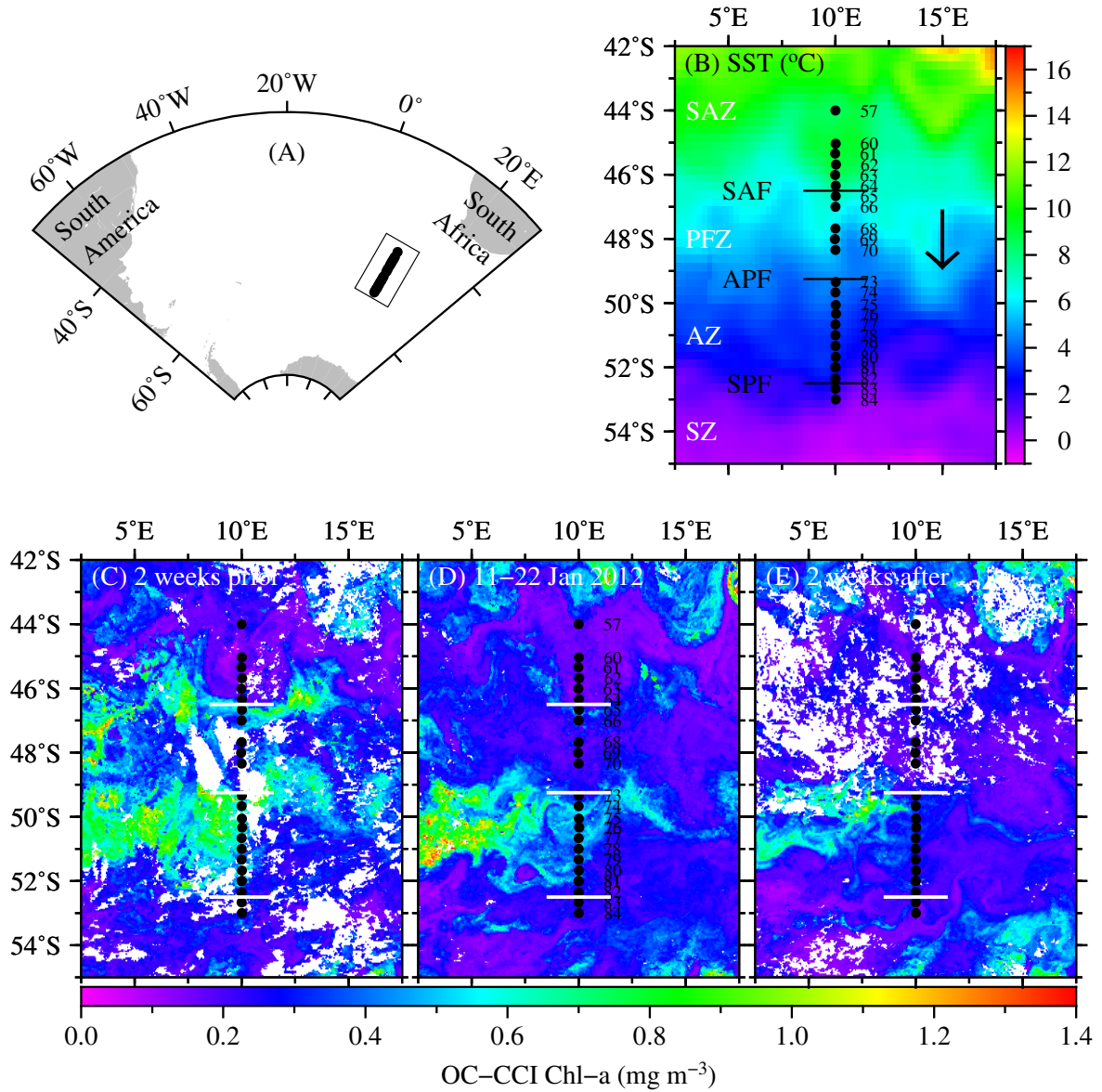


Figure 1: (A) Map showing the location of the sampling transect southwest of South Africa (inside the rectangle symbol) in the Atlantic sector of the Southern Ocean. (B) 12-day composite images of AVHRR sea surface temperature (°C) during the sampling from 11-22 January 2012. Composite images of daily OC-CCI Chl-a showing the transition of the phytoplankton bloom, (C) two weeks prior to cruise, (D) during the cruise period from 11 January to 22 January 2012, and (E) two weeks after the cruise. Black arrow in (B) shows the direction of the cruise track. Black circles in (B-E) are the sampling stations. White lines in (C-E) are oceanic front positions as in (B). Sub-Antarctic Front (SAF), Antarctic Polar Front (APF), Southern Polar Front (SPF) are the major oceanic fronts observed during the cruise. SAZ, Sub-Antarctic Zone; PFZ, Polar Front Zone; AZ, Antarctic Zone; SZ, Southern Zone

116 irradiance in the mixed layer (\bar{E}_{ML}) was calculated as: $\bar{E}_{ML} = \bar{E}_o [1 - e^{(-k_d \cdot z_{ML})}] / k_d \cdot z_{ML}$ (Boyd

117 et al., 2007; Cheah et al., 2013). \bar{E}_o is the 4 km daily surface PAR obtained from MODIS-
118 Aqua sensor.

119 2.3. Nutrients

120 NO_3+NO_2 , PO_4 and $\text{Si}(\text{OH})_4$ were measured colorimetrically using a Technicon TRAACS
121 800 auto-analyzer (Seal Analytical) on board the ship (Hoppe et al., this issue). DFe concen-
122 trations were determined onboard in a trace-metal clean condition according to the voltam-
123 metric method based on the electroactivity of iron complexed to dihydroxynaphthalene
124 (Laglera et al., 2013; Puigcorb  et al., this issue).

125 2.4. Pigment, community structure, and absorption

126 Water samples (1-2 L) were collected from one to seven depths within the upper 100 m
127 and filtered under low pressure (< 20 kPa) onto 25-mm Whatman GF/F filters. Filtered
128 samples were then immediately shock-frozen in liquid nitrogen and stored at -80°C until
129 analysis. Extraction and analysis of pigments were carried out based on the method of
130 Barlow et al. (1997) with modification customised to our instruments. In brief, pigments were
131 extracted in 1.5 mL 100% acetone plus 50 μL of canthaxanthin as internal standard solution
132 by homogenisation and centrifugation. Samples were analysed using a combination of a
133 Waters 717plus autosampler, a Waters 600 controller, a LC Microsorb C8 column (100 x 4.6
134 mm, 3 μm), and a Waters 2998 photodiode array detector. Identification and quantification
135 of pigments were carried out by comparing their retention times and absorption spectra
136 using the EMPOWER software provided by Waters. Part of pigment data were reported
137 in Soppa et al. (2014) and are publicly available at [http://doi.pangaea.de/10.1594/](http://doi.pangaea.de/10.1594/PANGAEA.848591)
138 [PANGAEA.848591](http://doi.pangaea.de/10.1594/PANGAEA.848591).

139 Phytoplankton community structure was calculated using the CHEMTAX program (Mackey
140 et al., 1996). The initial pigment ratios matrix as in Higgins et al. (2011) was applied to
141 estimate ten taxa that generally occur in the SAZ and PFZ. The taxa were cyanobacteria,
142 chlorophytes, prasinophytes, cryptophytes, diatoms-1 (contain Chl- c_1 , $-c_2$, and fucoxanthin),
143 diatoms-2 (Chl- c_1 was replaced by Chl- c_3 , typified by *Pseudonitzschia* sp.), dinoflagellates-
144 1 (contain unambiguous marker pigment peridinin), dinoflagellates-2 (containing fucoxan-
145 thin derivatives), haptophytes-6 (typified by *Emiliana* sp.), and haptophytes-8 (typified by
146 *Phaeocystis* sp.). Data were split into three bins according to sample depth to allow for vari-
147 ation of pigment ratios according to irradiance. The depth bins were 0-21 m ($n=41$), 22-61
148 m ($n=32$), and 61-100 m ($n=36$). Each bin was processed separately using the CHEMTAX
149 program.

150 In addition, the contribution (%) of three pigment-based phytoplankton size classes
151 (micro-, nano-, and picophytoplankton) to total phytoplankton biomass was estimated
152 following the method of Uitz et al. (2009). Microphytoplankton (micro) correspond to
153 phytoplankton with size >20 μm , nanophytoplankton (nano) between 2 to 20 μm , and
154 picophytoplankton (pico) between 0.2 to 2 μm . Fucoxanthin (Fuco), peridinin (Peri),
155 19'-hexanoyloxyfucoxanthin (Hex-fuco), 19'-butanoyloxyfucoxanthin (But-fuco), alloxanthin
156 (Allo), zeaxanthin (Zea), and monovinyl chlorophyll-b (MVChl-b, divinyl chlorophyll-b was
157 not detected in the samples) were the seven pigments chosen as diagnostic pigments (DP)

158 representing specific phytoplankton taxa and grouped into one of the three size classes in
159 the following equations:

160

$$161 \text{ micro (\%)} = 100 * ((1.41 * \text{Fuco}) + (1.41 * \text{Peri}) / \sum \text{DP})$$

$$162 \text{ nano (\%)} = 100 * ((1.27 * \text{Hex-fuco}) + (0.35 * \text{But-fuco}) + (0.60 * \text{Allo}) / \sum \text{DP})$$

$$163 \text{ pico (\%)} = 100 * ((0.86 * \text{Zea}) + (1.01 * \text{MVChl-b}) / \sum \text{DP})$$

164

165 in which $\sum \text{DP}$ represents the weighted sum of the concentrations of the seven diagnos-
166 tic pigments as in:

167

$$168 \sum \text{DP} = 1.41 * \text{Fuco} + 1.41 * \text{Peri} + 1.27 * \text{Hex-fuco} + 0.35 * \text{But-fuco} + 0.60 * \text{Allo} + 0.86 * \text{Zea} +$$
$$169 1.01 * \text{MVChl-b}$$

170

171 Seawater from one to seven depths within the upper 100 m was filtered under low pres-
172 sure (< 20 kPa) onto 47-mm Whatman GF/F filters. Filtered samples were then imme-
173 diately shock-frozen in liquid nitrogen and stored at -80°C until analysis. Measurements
174 for particulate [a_p (λ), m^{-1}] and detrital [a_d (λ), m^{-1}] absorption were carried out using
175 a Cary 4000 UV/VIS dual beam spectrophotometer equipped with a 150 mm integrating
176 sphere (Varian Inc., USA) as described in Taylor et al. (2011). Phytoplankton absorption
177 [a_{ph} (λ), m^{-1}] was obtained as the difference between the a_p and a_d . Part of phytoplank-
178 ton absorption data were reported in Soppa et al. (2013) and are publicly available at
179 <http://doi.pangaea.de/10.1594/PANGAEA.819617>.

180 2.5. Fast repetition rate fluorometry

181 Vertical profiles of chlorophyll fluorescence parameters of photosystem II (PSII) were
182 measured using a FASTtracka fast repetition rate fluorometer (FRRf, Chelsea Technology
183 Group, UK) attached to an optical cast. The optical cast also consisted of a 2π 400-700 nm
184 integrated PAR sensor, and a pressure sensor (all from Chelsea Technology Group, UK),
185 and a RAMSES ACC-VIS hyperspectral radiometer (TriOS GmbH, Germany) measuring
186 downwelling irradiance. The FRRf was programmed to deliver flash sequences consisting of
187 a series of 100 subsaturation flashlets at 1.1 μs duration and 2.8 μs intervals followed by a
188 series of 20 relaxation flashlets (1.1 μs flash duration and 51.6 μs intervals). Fluorescence
189 transients were then fitted to the biophysical model of Kolber et al. (1998) to yield values
190 of minimum fluorescence (F_o), maximum fluorescence (F_m) and effective absorption cross
191 section of PSII ($\sigma_{\text{PSII},478}$). To differentiate parameters measured during the day from dark-
192 adapted values, a prime (') symbol was added to the parameters measured during the day
193 (e.g. $\sigma_{\text{PSII},478}'$ vs. $\sigma_{\text{PSII},478}$). Minimum and maximum fluorescence at three stations i.e. at
194 47°S , 49.3°S , and 52°S , were corrected for background fluorescence based on the averaged
195 values of blank measurements obtained from filtered seawater (0.2 μm) collected at three
196 depths (10 m, Chl-a maximum, 100 m). Blank samples were not available for other stations.
197 The averaged values of the background fluorescence were $< 12\%$ of pre-corrected fluores-
198 cence values. Values of $\sigma_{\text{PSII},478}'$ were adjusted to the in situ light spectrum according to the
199 method of Suggett et al. (2006) as

200
201 $\sigma_{\text{PSII}'} = \sigma_{\text{PSII},478'}[\bar{a}(\text{in situ})]/[\bar{a}(\text{FRRf})]$
202
203 $\bar{a}(\text{FRRf})$ and $\bar{a}(\text{in situ})$ refer to the effective absorption coefficient determined from spec-
204 trally resolved a_{ph} , and excitation of FRRf LEDs and in situ downwelling irradiance, re-
205 spectively (Suggett et al., 2006). For stations without a_{ph} measurements, $\sigma_{\text{PSII},478}'$ values
206 were converted to $\sigma_{\text{PSII}'}$ based on the equation derived from the relationship between the
207 ratio of $\bar{a}(\text{FRRf}):\bar{a}(\text{in situ})$ and optical depth (ζ) (Fig. 2) as in $\sigma_{\text{PSII}'}(z) = \sigma_{\text{PSII},478}'(z)/[1.364$
208 $\exp^{-0.032\zeta}]$. Non-photochemical quenching (NPQ), defined as the ratio of total non-photochemical
209 dissipation to the rate constant for photochemistry in the light-adapted state was determined
210 based on the normalised Stern-Volmer (NPQ_{NSV}) coefficient as: NPQ_{NSV} = $(F_m'/F_v')-1$
211 = F_o'/F_v' (McKew et al., 2013). NPQ_{NSV} differs from the Stern-Volmer coefficient (F_m-
212 F_m'/F_m') that required both dark- and light-adapted F_m values (Olaizola et al., 1994),
213 which does not resolve the important differences between downregulation of excitation en-
214 ergy transfer in high light- and low light-adapted cells (McKew et al., 2013). NPQ_{NSV}
215 resolves these differences and is appropriate for our data set.

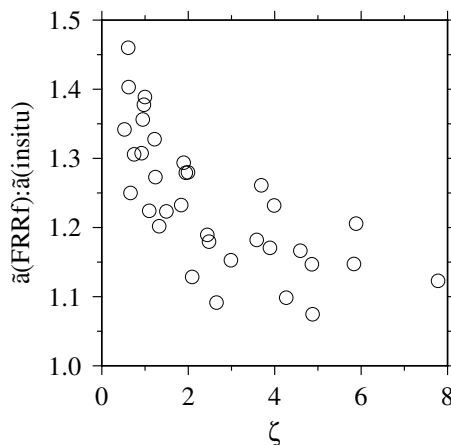


Figure 2: The relationship between the ratio of $\bar{a}(\text{FRRf}):\bar{a}(\text{in situ})$ and optical depth (ζ).

216 2.6. Statistical analysis

217 Mann-Whitney U-test was employed to test the differences in parameters between sta-
218 tions north and south of the APF. Relationships between biological and environmental
219 variables were examined using Spearman rank correlation analysis. All statistical analyses
220 were conducted with the statistical computing software "R" (R Core Team, 2014).

221 3. Results

222 3.1. Hydrography

223 The hydrography along the 10°E transect is discussed in detail by Strass et al. (this
224 issue). Here we summarize some of their results that are relevant in the current context.

225 Temperature in the upper 120 m ranged from 0.16 to 9.38°C (Fig. 3A) with a poleward
 226 decreasing trend. Three fronts were crossed: the Sub-Antarctic Front (SAF) at 46.5°S
 227 (indicated by a sharp drop in temperature from 8 to 6°C), the Antarctic Polar Front (APF)
 228 at 49.25°S, and the Southern Polar Front (SPF) at 52.5°S (Fig. 3). Mixed layer depths
 229 (z_{ML}) varied from 29 to 118 m with a large variation north of the APF; the shallowest and
 230 deepest z_{ML} were observed in the SAZ and PFZ, respectively (Fig. 3B). South of the APF,
 231 z_{ML} ranged from 43 to 107 m with a southward shoaling trend. z_{ML} was not significantly
 232 different between the stations north and south of the APF (Table 1).

233 3.2. Radiation

234 The depth of the euphotic zone (z_{eu}) ranged from 46 to 88 m along the transect and was
 235 significantly larger in waters north than south of the APF (Fig. 3B, Table 1). Along the
 236 transect, z_{ML} was mostly larger than z_{eu} in the AZ south of the APF and at stations with
 237 large z_{ML} . The ratios of z_{eu}/z_{ML} , where values below 1 indicate mixed waters and values
 238 above 1 indicating stratified waters (Uitz et al., 2008), were higher in the north (1.05 ± 0.50)
 239 than south (0.75 ± 0.37) of the APF, although the differences were not significant (Table
 240 1).

Table 1: Mean values and Mann-Whitney U-test of the differences between parameters in the north and south of the APF. Significant differences are indicate in **bold**. sd, standard deviation; ns, not significant.

Parameters	North of APF		South of APF		Mann-Whitney U-test p
	mean \pm sd	n	mean \pm sd	n	
z_{ML}	80.7 \pm 29.3	8	80.3 \pm 19.8	12	0.758 (ns)
z_{eu}	72.8 \pm 8.0	8	53.8 \pm 8.2	12	< 0.001
z_{eu}/z_{ML}	1.05 \pm 0.50	8	0.75 \pm 0.37	12	0.070 (ns)
\bar{E}_o	47.5 \pm 13.3	8	55.0 \pm 6.6	12	0.231 (ns)
\bar{E}_{ML}	10.4 \pm 4.8	8	8.8 \pm 4.0	12	0.375 (ns)
NO ₃ +NO ₂	16.4 \pm 3.2	85	23.4 \pm 1.3	75	< 0.001
PO ₄	1.21 \pm 0.19	85	1.57 \pm 0.10	75	< 0.001
Si(OH) ₄	1.83 \pm 1.16	85	17.21 \pm 9.36	75	< 0.001
DFe	0.15 \pm 0.08	8	0.13 \pm 0.06	16	0.839 (ns)
TChl-a	0.37 \pm 0.12	51	0.66 \pm 0.31	58	< 0.001
^a (DD+DT)/TChl-a	0.20 \pm 0.04	27	0.17 \pm 0.04	34	0.021
^a DD+DT	0.08 \pm 0.03	27	0.11 \pm 0.04	34	< 0.001
^a Incident PAR	36.6 \pm 52.6	590	181.9 \pm 212.2	547	< 0.001
F_v/F_m	0.33 \pm 0.03	68	0.36 \pm 0.04	188	< 0.001
F_v/F_o	0.49 \pm 0.07	68	0.57 \pm 0.10	188	< 0.001
σ_{PSII}	6.59 \pm 0.68	68	5.93 \pm 0.70	188	< 0.001
$1/\tau_{Qa}$	0.17 \pm 0.19	68	0.24 \pm 0.08	188	< 0.001

^a Only data from upper 50 m were included to avoid the influence of low irradiance at deeper depth.

241 Daily surface PAR (\bar{E}_o) was ~ 50 mol photons $m^{-2} d^{-1}$ in the SAZ and dropped to ~ 30
 242 mol photons $m^{-2} d^{-1}$ in the PFZ. In the AZ, \bar{E}_o increased to ~ 55 mol photons $m^{-2} d^{-1}$
 243 (Fig 3B). On average, \bar{E}_o was not significantly different north and south of the APF (Table
 244 1). Total daily irradiance in the mixed layer (\bar{E}_{ML}) ranged between 3.9 to 17.5 mol photons
 245 $m^{-2} d^{-1}$) along the transect whereby $\bar{E}_{ML} > 10$ mol photons $m^{-2} d^{-1}$ have been observed
 246 at stations both north and south of the APF (Fig. 3B). Mean \bar{E}_{ML} values were 10.4 ± 4.8
 247 in waters north of the APF and 8.8 ± 4.0 in the south of the APF. High \bar{E}_{ML} were generally
 248 recorded at stations with shallower z_{ML} . No significant differences were observed between
 249 \bar{E}_o values recorded north and south of the APF (Table 1).

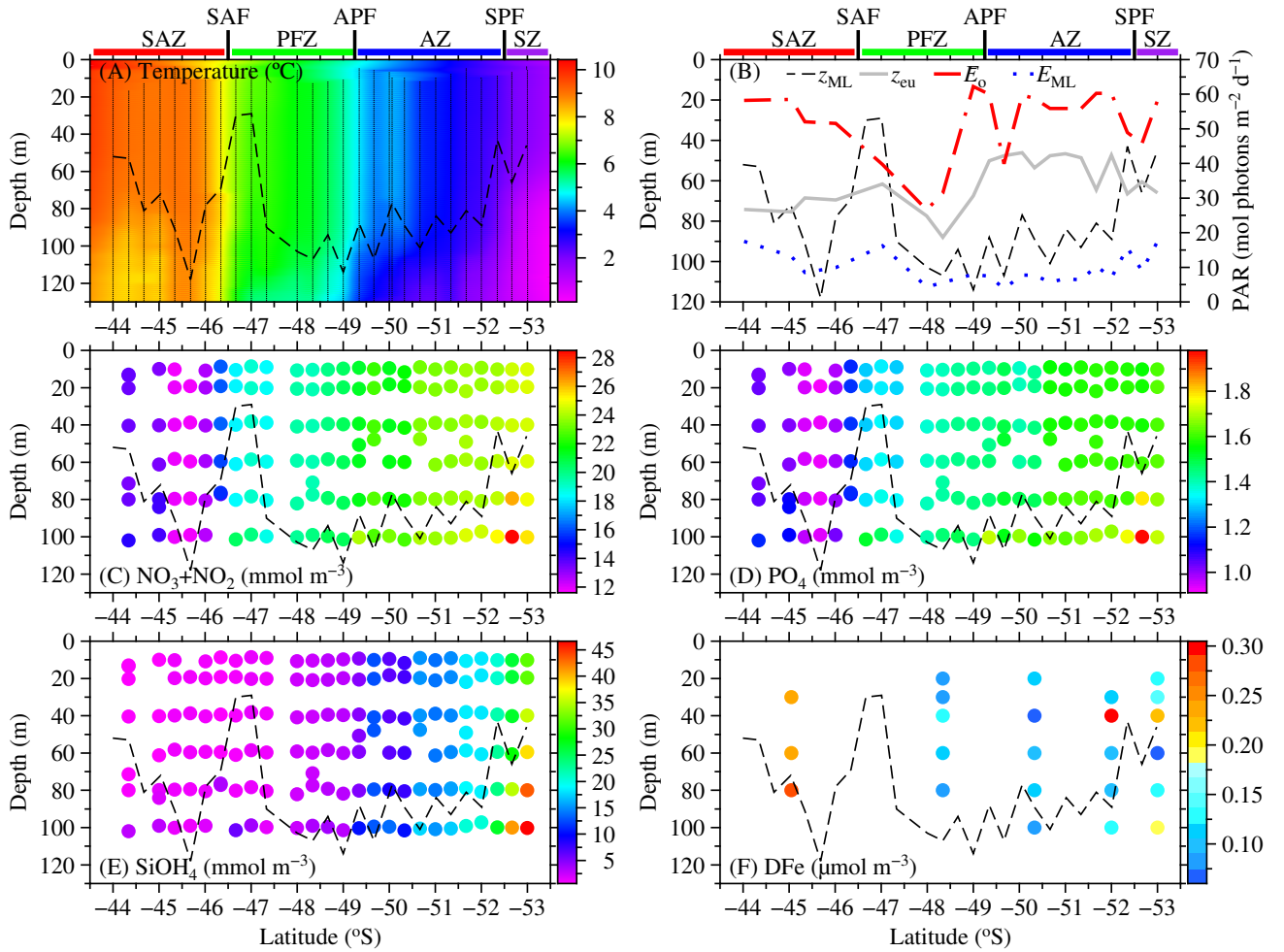


Figure 3: Vertical structures of (A) temperature, (B) mixed layer depth (z_{ML}), euphotic depth (z_{eu}), daily surface PAR (\bar{E}_o), and total daily irradiance in the mixed layer (\bar{E}_{ML}), (C) nitrate+nitrite, (D) phosphate, (E) silicic acid, and (F) dissolved iron along the $10^\circ E$ transect. Black dotted lines in panels (A) and (C-F) indicate z_{ML} as in panel (B). SAF, Sub-Antarctic Front; APF, Antarctic Polar Front; SPF, Southern Polar Front; STZ, Sub-Tropical Zone; SAZ, Sub-Antarctic Zone; PFZ, Polar Frontal Zone; AZ, Antarctic Zone.

250 Concentrations of NO_3+NO_2 within the upper 100 m were always > 11.5 $mmol m^{-3}$

251 along the transect (Fig. 3C). Although concentrations of NO_3+NO_2 were replete across the
 252 whole transect, a sharp increase from north to south in NO_3+NO_2 can clearly be observed
 253 across all three fronts i.e. SAF, APF, and SPF. NO_3+NO_2 concentrations in waters south
 254 of the APF were significantly higher than those in waters north of the APF with mean
 255 values of $23.4 \pm 1.3 \text{ mmol m}^{-3}$ and $16.4 \pm 3.2 \text{ mmol m}^{-3}$, respectively (Table 1). The
 256 vertical structure of NO_3+NO_2 within the upper 100 m was very uniform except in the
 257 Southern Zone (SZ) in which NO_3+NO_2 concentrations were higher below the mixed layer.
 258 PO_4 concentrations ranged from 0.92 to 1.98 mmol m^{-3} with similar spatial and vertical
 259 distributions as NO_3+NO_2 and higher concentrations observed further south (Fig. 3D).
 260 The region with slightly lower concentrations in PO_4 ($\sim 0.9 \text{ mmol m}^{-3}$) coincides with lower
 261 NO_3+NO_2 concentrations ($\sim 11.8 \text{ mmol m}^{-3}$) at 45.3°S - 46°S in the SAZ. Concentrations of
 262 $\text{Si}(\text{OH})_4$ exhibit a distinctive pattern across the APF. In waters north of the APF, $\text{Si}(\text{OH})_4$
 263 concentrations were depleted with a mean concentration of only $1.83 \pm 1.16 \text{ mmol m}^{-3}$ (Table
 264 1). At the APF, concentrations of $\text{Si}(\text{OH})_4$ increased to $\sim 5 \text{ mmol m}^{-3}$ (Fig. 3E). South
 265 of the APF, $\text{Si}(\text{OH})_4$ concentrations were much higher with a mean concentration of 17.21
 266 $\pm 9.36 \text{ mmol m}^{-3}$. $\text{Si}(\text{OH})_4$ concentrations were generally uniform within the mixed layer.
 267 Concentrations of dissolved iron (DFe) within the upper 100 m were typically low across
 268 the whole transect varying between 0.060 to 0.305 $\mu\text{mol m}^{-3}$ (Fig. 3F). Strong depletion in
 269 DFe concentrations ($< 0.12 \mu\text{mol m}^{-3}$) was observed in waters close to the APF, between
 270 south of the PFZ and north of the AZ (48°S - 51°S). DFe concentrations $> 0.2 \mu\text{mol m}^{-3}$ were
 271 recorded in the SAZ, south of the AZ, and in the SZ. As with NO_3 , concentrations of PO_4
 272 and $\text{Si}(\text{OH})_4$ were significantly higher at stations south of the APF than north of the APF,
 273 whereas DFe concentrations were not significantly different between the stations (Table 1).

274 3.3. Phytoplankton pigment and community composition

275 Along the 10°E transect, TChl-a concentrations within the upper 100 m ranged from
 276 0.07 to 1.31 mg m^{-3} (Fig. 4A) with mean TChl-a concentration in waters north of the APF
 277 ($0.37 \pm 0.12 \text{ mg m}^{-3}$) only half and significantly lower than the mean TChl-a concentration
 278 in waters south of the APF ($0.66 \pm 0.31 \text{ mg m}^{-3}$, Table 1). In the SAZ and PFZ north of
 279 the APF, concentrations of TChl-a were typically between 0.2-0.4 mg m^{-3} except at 45.3°S
 280 and 47°S , where the TChl-a concentrations were higher with 0.5 mg m^{-3} and 0.8 mg m^{-3} ,
 281 respectively. South of the APF, TChl-a concentrations were mostly higher than 0.5 mg
 282 m^{-3} except in the SZ (Fig. 4A). TChl-a concentrations $> 1 \text{ mg m}^{-3}$ were confined to the
 283 AZ south of the APF at around 49.7°S , and between 50.3°S and 51.3°S , where z_{ML} was
 284 larger than z_{eu} . Significant negative correlation was observed between between TChl-a and
 285 $z_{\text{eu}}/z_{\text{ML}}$ ratio (Table 2), indicating that phytoplankton blooms were confined to well-mixed
 286 waters. The correlation between 100 m-integrated TChl-a and $\text{Si}(\text{OH})_4$ was not significant,
 287 due mainly to low TChl-a concentrations in the SZ (Fig. 4A). However, when data from
 288 the SZ was excluded, a significant positive correlation between TChl-a and $\text{Si}(\text{OH})_4$ was
 289 obtained (Table 2).

290 A distinctive phytoplankton community structure was observed north and south of the
 291 APF (Fig. 4B). North of the APF, dominance of haptophytes up to 90% was recorded
 292 in the north of the SAZ. Contribution of haptophytes gradually reduced southward but it

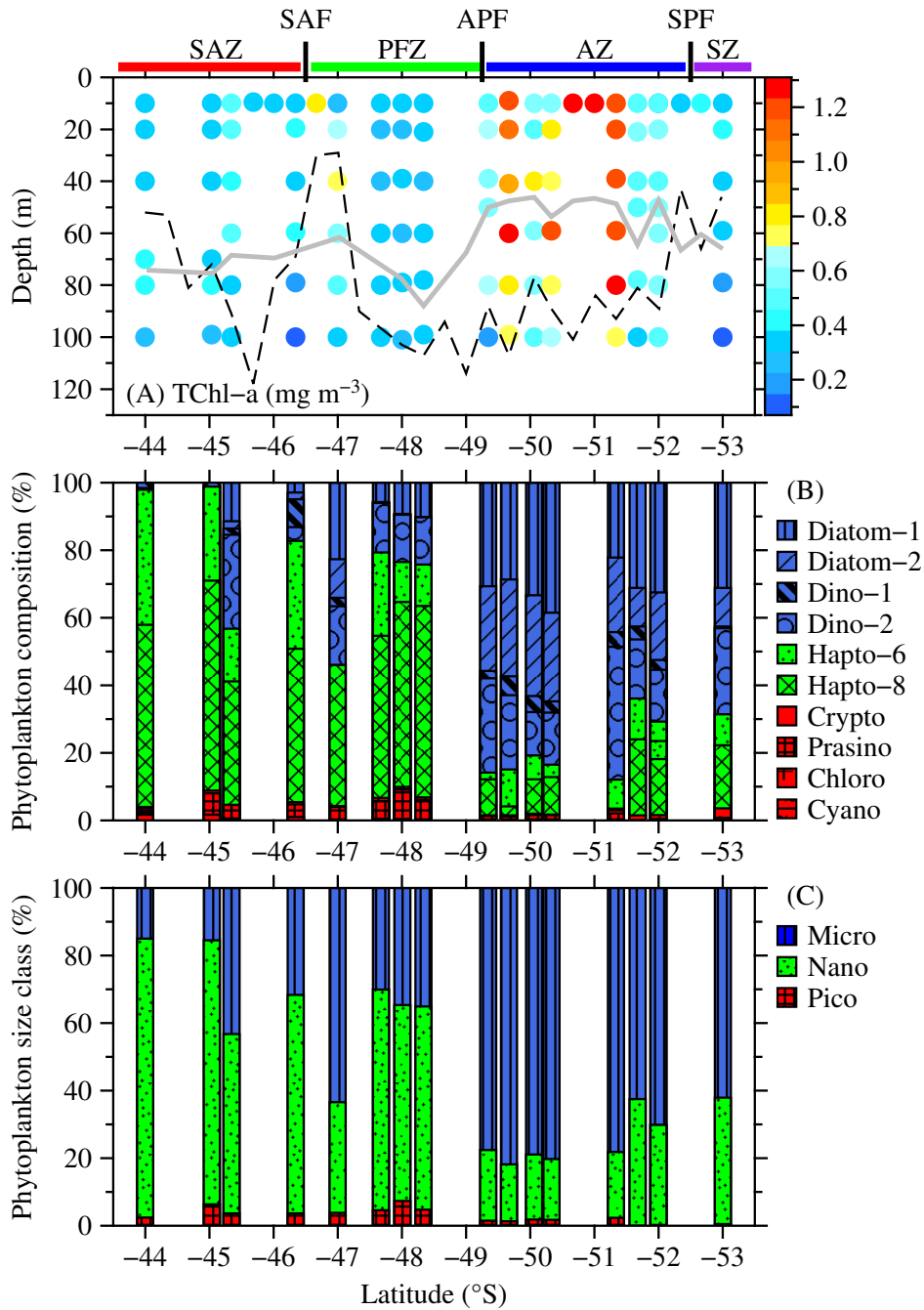


Figure 4: (A) TChl-a concentrations, relative contribution (%) of 100-m integrated (B) phytoplankton taxa, and (C) size classes along the transect. Black dotted line and grey solid line in panel (A) indicate z_{ML} and z_{eu} , respectively. SAF, Sub-Antarctic Front; APF, Antarctic Polar Front; SPF, Southern Polar Front; STZ, Sub-Tropical Zone; SAZ, Sub-Antarctic Zone; PFZ, Polar Frontal Zone; AZ, Antarctic Zone; SZ, Southern Zone.

293 maintained a strong dominance of $\sim 70\text{-}80\%$ in the PFZ except at 45.3°S and 47°S , where
294 the contribution of haptophytes dropped to about $40\text{-}50\%$. Coincidentally, these two stations
295 also reported an increase in TChl-a concentration (Fig. 4A) and the highest contribution
296 of diatoms ($13\text{-}24\%$) and dinoflagellates-2 ($20\text{-}29\%$, heterotrophic) in waters north of the
297 APF (Fig. 4B). At taxa level, waters north of the APF were dominated by *Phaeocystis*
298 sp. as indicate by a high contribution of haptophytes-8. South of the APF, diatoms-1
299 was the dominant group contributing about $22\text{-}39\%$ of total biomass, followed by diatoms-2
300 ($\sim 11\text{-}30\%$, typified by *Pseudonitzschia* sp.) and heterotrophic dinoflagellates-2 ($\sim 6\text{-}40\%$).
301 Vertical profiles of phytoplankton community structure show at stations south of the APF,
302 dominance of diatoms-2 (*Pseudonitzschia* sp.) widespread within the 100 m water column
303 (Fig. 5B). A similar distribution was observed for dinoflagellates-1 (Fig. 5C). In contrast,
304 the vertical distribution of haptophytes-8 shows higher contribution at the surface than at
305 depth in the north of the APF (Fig. 5F). Contribution of prasinophytes were higher in the
306 PFZ than in other zones (Fig. 5G).

307 Distribution of pigment-based phytoplankton size classes exhibits similar trends as in
308 phytoplankton groups with nanophytoplankton dominating north of the APF and waters
309 south of the APF were dominated by macrophytoplankton (Fig. 4C). Overall, cyanobac-
310 teria and picophytoplankton contribute less than 10% of total biomass along the tran-
311 sect. Contrasting relationships were obtained between different phytoplankton size classes
312 and macronutrients (Table 2). As expected, positive correlations were obtained between
313 macronutrients and microphytoplankton and negative with nano- and picophytoplankton,
314 suggesting that macronutrients were driving the succession of bigger cells along the transect.
315 Two types of Chl-a degraded products, chlorophyllide-a and pheophorbide-a, were observed
316 in this study. High ratios of chlorophyllide-a/TChl-a were observed at all high TChl-a
317 stations along the transect (Fig. 6A), whereas ratios of pheophorbide-a/TChl-a were only
318 recorded at high TChl-a stations south of the APF (Fig. 6B).

319 3.4. Photoprotective pigments

320 Ratios of the photoprotective xanthophyll cycle pigments, diadinoxanthin (DD) + di-
321 atoxanthin (DT)/TChl-a ((DD+DT)/TChl-a) were generally higher at the surface and
322 ranged from 0.12 to 0.28 within the upper 20 m (Fig. 6C). A more profound decrease
323 in (DD+DT)/TChl-a ratios below the mixed layer was observed at stations with shal-
324 lower mixed layer than at those with deep mixed layer. At the deep mixed layer stations,
325 (DD+DT)/TChl-a ratios higher than 0.10 can be observed down to $80\text{-}100$ m along the
326 transect. The different vertical patterns in (DD+DT)/TChl-a ratios reflect the influence
327 of water stratification on photoacclimation strategy of phytoplankton. (DD+DT)/TChl-a
328 ratios in waters north of the APF were significantly higher than those in the south (Table
329 1). High ratios of (DD+DT)/TChl-a in waters north of the APF were due to low TChl-a
330 as DD+DT concentrations were significantly higher in waters south of the APF (Table 1).
331 There was a significant negative correlation between (DD+DT)/TChl-a and microphyto-
332 plankton, and a significant positive correlation with nanophytoplankton along the transect
333 indicating that nanophytoplankton, in particular haptophytes, were producing more photo-
334 protective pigments and less TChl-a than macrophytoplankton.

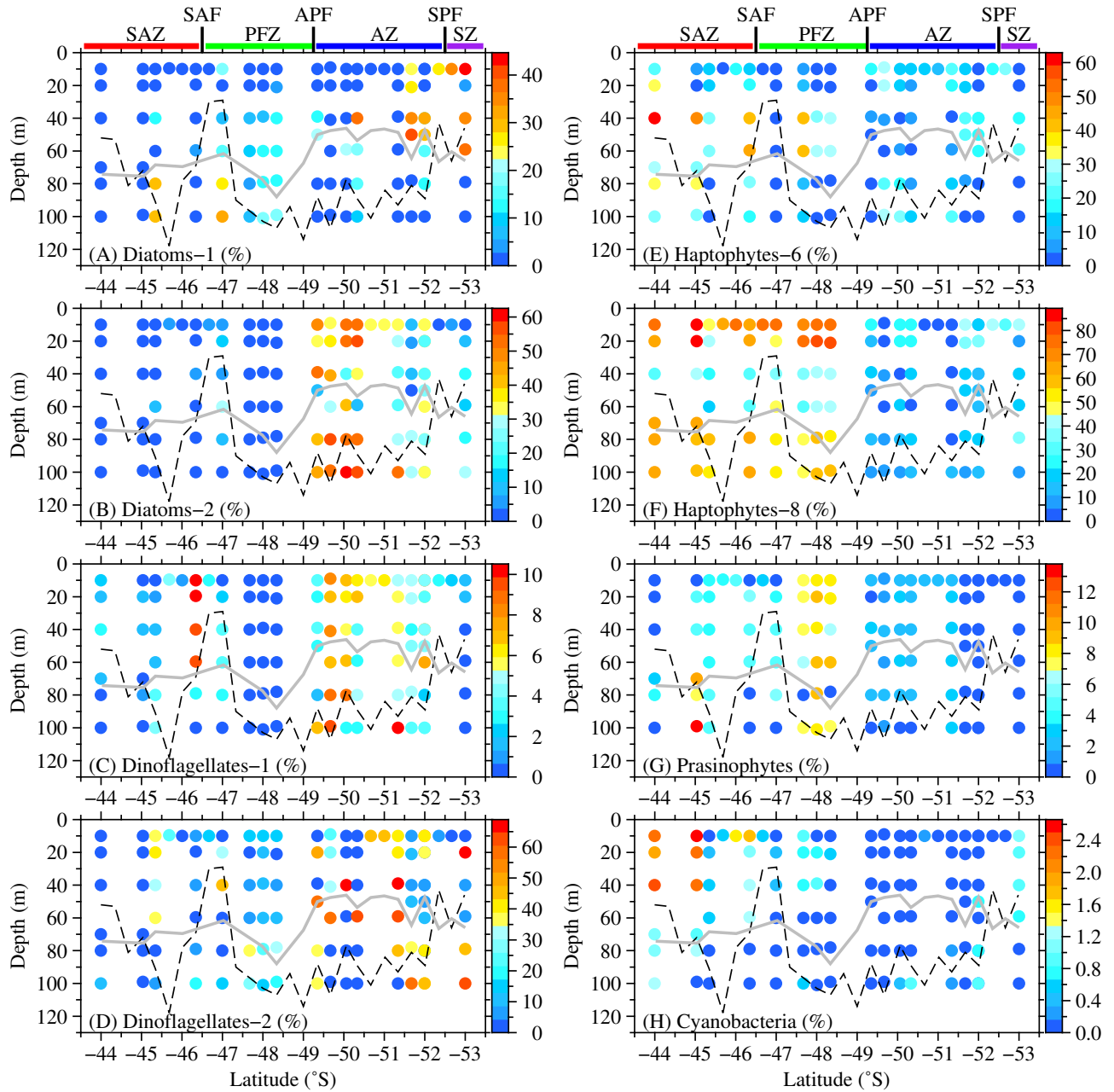


Figure 5: (A) Vertical structures of relative contribution (%) of major phytoplankton taxa along the transect. Black dotted lines and grey solid lines in all panels indicate z_{ML} and z_{eu} , respectively. SAF, Sub-Antarctic Front; APF, Antarctic Polar Front; SPF, Southern Polar Front; STZ, Sub-Tropical Zone; SAZ, Sub-Antarctic Zone; PFZ, Polar Frontal Zone; AZ, Antarctic Zone; SZ, Southern Zone.

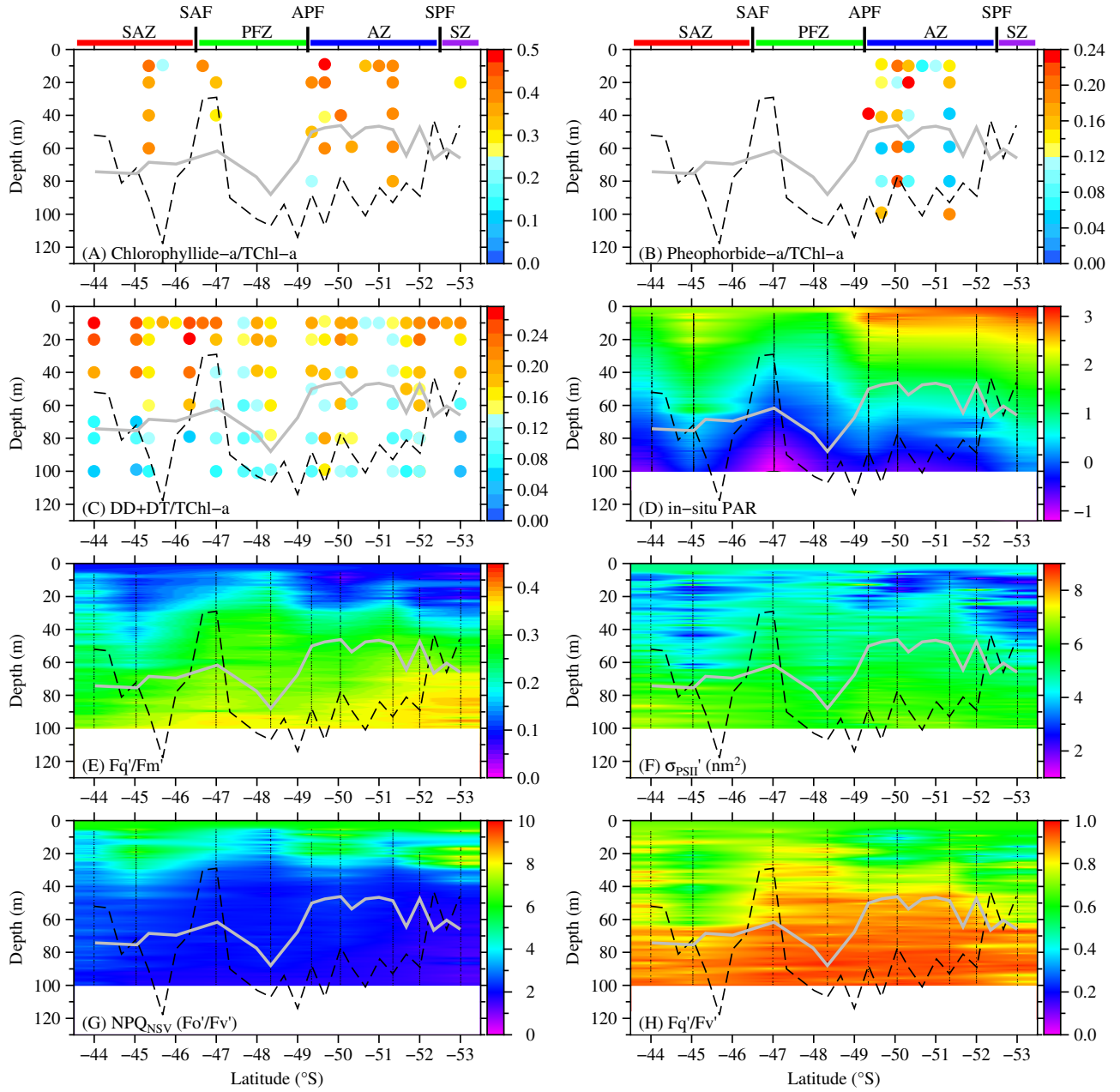


Figure 6: Vertical structures of the concentrations of Chl-a degraded products (A) chlorophyllide-a and (B) pheophorbide-a. (C) Total photoprotective pigments in the xanthophyll cycle ((DD+DT)/TChl-a). (D) Log(base 10)-transformed incident PAR ($\mu\text{mol photons m}^{-2} \text{s}^{-1}$). (E) Overall actual operating efficiency of PSII under ambient light (F'_q/F'_m) and (F) functional absorption cross section of PSII (σ'_{PSII}) under ambient light. Black dotted lines and grey solid lines in all panels indicate z_{ML} and z_{eu} , respectively. SAF, Sub-Antarctic Front; APF, Antarctic Polar Front; SPF, Southern Polar Front; STZ, Sub-Tropical Zone; SAZ, Sub-Antarctic Zone; PFZ, Polar Frontal Zone; AZ, Antarctic Zone; SZ, Southern Zone.

Table 2: Relationships between biological parameters and environmental properties for all stations. Significant correlations at 95% significance level are indicate in **bold**.

Parameters	All stations		
	<i>r</i>	<i>p</i>	<i>n</i>
^a TChl-a vs. z_{eu}/z_{ML}	-0.65	0.014	14
^a TChl-a vs. $Si(OH)_4$	0.275	0.341	14
^b TChl-a vs. $Si(OH)_4$	0.59	0.036	13
Microphytoplankton vs. NO_3+NO_2	0.55	< 0.001	83
Microphytoplankton vs. PO_4	0.57	0.000	83
Microphytoplankton vs. $Si(OH)_4$	0.52	< 0.001	83
Nanophytoplankton vs. NO_3+NO_2	-0.54	< 0.001	83
Nanophytoplankton vs. PO_4	-0.56	< 0.001	83
Nanophytoplankton vs. $Si(OH)_4$	-0.51	< 0.001	83
^c (DD+DT)/TChl-a vs. Microphytoplankton	-0.40	0.002	58
^c (DD+DT)/TChl-a vs. Nanophytoplankton	0.41	0.002	58
F_v/F_m vs. Microphytoplankton	0.31	0.003	25
F_v/F_m vs. Nanophytoplankton	-0.35	0.002	25
Dinoflagellates-2 vs. chlorophyllide-a	0.73	< 0.001	104
Haptophytes-8 vs. chlorophyllide-a	-0.40	< 0.001	104

^a100 m-integrated data.

^b100 m-integrated data from all stations except data from 53° in the SZ.

^cOnly data from upper 50 m were included to avoid the influence of low irradiance at deeper depth.

Table 3: Relationships between biological and environmental parameters in regions north and south of the APF. Significant correlations at 95% significance level are indicate in **bold**.

Parameters	North of APF			South of APF		
	<i>r</i>	<i>p</i>	<i>n</i>	<i>r</i>	<i>p</i>	<i>n</i>
^a NPQ _{NSV} vs. incident PAR	0.82	< 0.001	164	0.91	< 0.001	187
^a NPQ _{NSV} vs. (DD+DT)/TChl-a	0.76	0.016	10	0.57	0.200	7
^a (DD+DT)/TChl-a vs. incident PAR	0.72	0.011	12	0.61	0.024	14

^aOnly data from upper 50 m were included to avoid the influence of low irradiance at deeper depth.

335 3.5. Biophysical PSII parameters

336 The values of overall actual operating efficiency of PSII under ambient light (F'_q/F'_m)
337 varied from 0.01 to 0.44 in the upper 100 m, and were low (0.01-0.15) from the surface down
338 to around 30 m at most of the stations, reflecting the influence of high light at the surface.

339 At 48.3°S, due to low surface incident PAR (Fig. 6D), surface F'_q/F'_m values were around
340 0.20 (Fig. 6E). Below 30 m, F'_q/F'_m gradually increased with values ranging from 0.15 to
341 0.30 within the mixed layer. F'_q/F'_m higher than 0.35 were only observed either near the z_{ML}
342 or below the z_{ML} in which maximum F'_q/F'_m of 0.44 was observed below the z_{ML} at 95 m
343 at Station 84 (53°S) south of the APF (Fig. 6E). Maximum efficiency of PSII in the dark
344 (F_v/F_m) ranged from 0.23 to 0.49 with lower values at the surface (0.26-0.38) and increased
345 with depth reaching the maximum value of 0.49 at around 98 m at Station 81 (52°S, data
346 not shown). The mean F_v/F_m in waters north of the APF was 0.33 ± 0.03 which was
347 significantly lower than mean F_v/F_m value (0.36 ± 0.04) in waters south of the APF (Table
348 1). Mean F_v/F_o , which represents the proportion of functional PSII reaction centres (RCII),
349 was significantly higher in waters south of the APF (0.49 ± 0.07) than those in the north
350 of the APF (0.57 ± 0.10 ; Table 1).

351 The values of effective absorption cross section of PSII under ambient light (σ'_{PSII}) varied
352 from 1.17 to 8.89 nm² and showed similar vertical distribution as in F'_q/F'_m with low values
353 at the surface extending to 50 m within the mixed layer and increased below the mixed
354 layer (Fig. 6F). Effective absorption cross section of PSII in the dark (σ_{PSII}) ranged between
355 4.20-8.83 nm² with a significantly higher mean value in waters north of the APF than south
356 of the APF (Table 1). No significant correlations were observed between DFe, F_v/F_m and
357 σ_{PSII} along the transect. Incidentally, F_v/F_m were observed to correlate positively with
358 microphytoplankton and negatively with nanophytoplankton (Table 2). The rate constant
359 for reopening of closed RCII ($1/\tau_{Qa}$), determined from the inverse of the turnover time for
360 PSII, were significantly lower in waters north of the of APF (0.17 ± 0.19 ms⁻¹) than in the
361 south (0.23 ± 0.08 ms⁻¹, Table 1).

362 High values of NPQ_{NSV} were observed at stations under the influence of high incident
363 PAR within the upper 50 m (Fig. 6D & G) in both north and south regions of the APF
364 (Table 3). Correspondingly, significant positive correlations were also obtained between
365 (DD+DT)/TChl-a and incident PAR in both regions across the APF. This is expected
366 given the photoprotective role of the xanthophyll cycle pigments in dissipating excessive
367 energy under high irradiance condition via non-photochemical quenching. Interestingly,
368 only the region north of the APF shows significant positive correlation between NPQ_{NSV}
369 and (DD+DT)/TChl-a (Table 3), although high NPQ_{NSV} values were recorded across the
370 whole transect. In contrast to NPQ_{NSV}, values of F'_q/F'_v , which accounts for the proportion
371 of RCII in the “open” state, were low at the surface and increased at further depth when
372 the influence of PAR is negligible (Fig. 6H).

373 4. Discussion

374 4.1. State of the phytoplankton bloom

375 Although TChl-a concentrations > 1 mg m⁻³ can be observed in waters south of the
376 APF, satellite images before and after the cruise show that the phytoplankton bloom was
377 at a declining stage during sampling. High concentrations of degraded Chl-a products, i.e.
378 chlorophyllide-a and pheophorbide-a at high TChl-a stations indicate a declining bloom
379 (Wright et al., 2010). Chlorophyllide-a and pheophorbide-a can be produced from senesced

380 phytoplankton or by mastication during grazing (Louda et al., 1998; Wright et al., 2010).
381 The high contribution of dinoflagellates-2 observed only at high TChl-a stations (Fig. 4A),
382 suggests that grazing activity by heterophic dinoflagellates was taking place at these sta-
383 tions (Fig. 4B). It should be noted that dinoflagellates-2 lack unique diagnostic pigments
384 and contain Fuco and Hex-fuco as their main carotenoids, which are shared by a number
385 of taxa, notably haptophytes (Wright et al., 2010; de Salas et al., 2011). Nevertheless, a
386 significant positive correlation was observed between chlorophyllide-a and dinoflagellates-2,
387 and a negative correlation between chlorophyllide-a and haptophytes-8 (Table 2), indicating
388 that chlorophyllide-a concentrations at high TChl-a stations were not contributed by haptophytes.
389 High concentrations of heterotrophic flagellates have also been reported across the
390 SAZ and PFZ in the Southern Pacific Ocean (de Salas et al., 2011), which are one of the
391 major grazers in those regions (Pearce et al., 2011).

392 4.2. Indications of iron limitation

393 With a maximum achievable F_v/F_m value of ca. 0.65 under optimal nutrient replete
394 conditions (Kolber and Falkowski, 1993), low mean F_v/F_m (< 0.40) values observed across
395 the north and south regions of the APF could be attributed to iron limitation. Low mean
396 values of $1/\tau_{Qa}$ ($< 0.3 \text{ ms}^{-1}$) across the APF suggest that there was a large proportion of
397 reduced plastoquinone pool (McKew et al., 2013), which could have resulted from a large
398 proportion of reduced RCII. Laboratory and ship-board iron fertilisation experiments have
399 reported an increase in F_v/F_m to > 0.5 and $1/\tau_{Qa} > 0.3 \text{ ms}^{-1}$ in response to iron addition
400 (Greene et al., 1992; Kolber et al., 1994; Moore et al., 2007). Studies have shown that
401 diatoms are capable of coping with low iron conditions by reducing the concentrations of iron-
402 demanding cellular components such as cytochrome b_6f (cyt b_6f) and photosystem I (PSI)
403 protein complexes, which are electron acceptors downstream of PSII (Greene et al., 1992;
404 Strzpek and Harrison, 2004). As a result, low concentrations of these electron acceptors
405 will result in a large proportion of RCII remaining in a reduced state, lowering F_v/F_m and
406 $1/\tau_{Qa}$ (Greene et al., 1992).

407 4.3. Phytoplankton assemblages under low and modest silicic acid concentrations

408 Under $\text{NO}_3+\text{NO}_2^-$, PO_4 -repleted, and DFe-limited conditions, $\text{Si}(\text{OH})_4$ plays a signifi-
409 cant role in controlling phytoplankton biomass and community structure across the APF
410 regions as indicated in the significant positive correlations between $\text{Si}(\text{OH})_4$, TChl-a, and
411 microphytoplankton. In waters north of the APF, mean $\text{Si}(\text{OH})_4$ concentration ($< 2 \text{ mmol}$
412 m^{-3}) showed that cells were suffering from $\text{Si}(\text{OH})_4$ deficiency (Franck et al., 2000). As
413 a consequence, $\text{Si}(\text{OH})_4$ limitation leads to the dominance of smaller nanophytoplankton
414 mainly haptophytes, which usually prevail over larger cells under $\text{Si}(\text{OH})_4$ limitation con-
415 dition (Hutchins et al., 2001). In contrast, sufficient supply of $\text{Si}(\text{OH})_4$ ($> 5 \text{ mmol m}^{-3}$)
416 in waters south of the APF lead to high TChl-a concentrations and diatoms dominated
417 phytoplankton community structure.

4.4. Influence of light in the shallow and deep mixed layer

The relatively weaker contrast in vertical distribution of (DD+DT)/TChl-a ratios within the mixed layer at stations with deeper mixed layer, i.e. $z_{ML} > z_{eu}$ shows that phytoplankton in well-mixed waters spent more time in the deeper parts of the mixed layer receiving less light. The corresponding higher values of σ'_{PSII} within the mixed layer and low \bar{E}_{ML} concentrations indicate that phytoplankton at these stations on average spent more time in a relatively low irradiance environment. This suggests that during the mixing process, phytoplankton at deep mixed layer stations were exposed to a range of irradiance intensities and acclimating to lower levels of irradiance. Laboratory experiments have shown that diatoms and haptophytes exposed to fluctuation in irradiance are acclimating to lower irradiances than cells grown under constant irradiance (van de Poll et al., 2007, 2009). This could explain the lower ratios of (DD+DT)/TChl-a to TChl-a at these stations. In contrast, phytoplankton at shallower mixed layer stations were trapped within a shallower and more stratified water column, and therefore were exposed to higher light intensity. Consequently, phytoplankton at these stations were producing more photoprotective pigments at the expense of Chl-a. Significant negative correlations between 100-m integrated TChl-a and z_{eu}/z_{ML} at all stations (Table 2), which shows that TChl-a concentrations were lower at shallower and more stratified stations, confirm that this is the case.

DD and DT are the main photoprotective xanthophyll cycle pigments widespread in diatoms, haptophytes and dinoflagellates. DD pigment will assist in light harvesting by transferring energy to chlorophylls under lower light condition, whereas under intense light, DD will be converted to DT to shield off excessive light energy via NPQ. The DD+DT xanthophyll cycle and NPQ operate as a rapid photoacclimation mechanism regulating between light harvesting and thermal dissipation of excess light energy under rapid light fluctuation conditions (Brunet and Lavaud, 2010; Goss and Jakob, 2010). Low values of F'_q/F'_m , F'_q/F'_v , and σ'_{PSII} in response to high incident PAR at the surface indicate that a large proportion of RCII were reduced. Large fraction of reduced RCII under high irradiance conditions have shown to increase the capacity of NPQ and reducing the risk of photodamage (Moore et al., 2006). Our results indicate that xanthophyll cycling and NPQ provide a cost-effective short-term photoprotection mechanisms that are vital to phytoplankton living in the iron-limited and rapid light fluctuation environment in the APF.

4.5. Contrasting photoacclimation response in haptophytes- and diatoms-dominated community

In the haptophytes-dominated region north of the APF, the ratios of (DD+DT)/TChl-a were significantly higher than in the south despite being exposed to lower incident PAR and similar \bar{E}_{ML} levels (Table 1). As DFe concentrations were not significantly different between the regions in the north and south of the APF, differences in the ratios of (DD+DT)/TChl-a may originate from taxon-specific response to light. Studies have shown that haptophytes are better adapted to low light and are more prone to photoinhibition compared to diatoms that are better acclimated to high light (Arrigo et al., 2000; Kropuenske et al., 2010). The study by Alderkamp et al. (2012) has also shown that haptophytes produced higher ratios of (DD+DT)/TChl-a than diatoms under iron-limited conditions. Similarly, significantly

460 lower F_v/F_m , F_v/F_o , $1/\tau_{Qa}$, and higher σ_{PSII} observed in the region north of the APF could
461 have been due to the high abundance of nanophytoplankton in this region. Phytoplankton
462 with smaller cell size have shown to exhibit lower F_v/F_m and higher σ_{PSII} than larger phyto-
463 plankton such as diatoms (Suggett et al., 2009). In this study, nanophytoplankton correlate
464 positively with (DD+DT)/TChl-a and negatively with F_v/F_m (Table 2), suggesting that
465 higher (DD+DT)/TChl-a ratios and lower F_v/F_m observed in the region north of the APF
466 may be due to the domination of smaller size phytoplankton in this region.

467 5. Conclusion

468 Our findings show that in addition to iron, other factors such as light, mixed layer
469 depth, Si(OH)_4 , and photoacclimation response of phytoplankton also play important roles
470 in regulating TChl-a concentrations in the APF. Overall, under iron-limited conditions,
471 phytoplankton across the APF were more prone to high light, especially for cells living in a
472 shallow mixed layer (< 60 m) environment and were producing more photoprotective pig-
473 ments at the expense of Chl-a. Across the APF, even though the influence of Si(OH)_4 was
474 confined to taxonomic level, the subsequent photoacclimation response of different phyto-
475 plankton groups driven by Si(OH)_4 , in turn, was influencing the concentrations of TChl-a in
476 the regions north and south of the APF. Based on our findings, we propose that high TChl-a
477 concentrations ($> 0.6 \text{ mg m}^{-3}$) are achievable even for iron-limited phytoplankton living in
478 the vicinity of the APF during late summer, if $z_{ML} > 60$ m, $z_{eu}/z_{ML} < 1$, and Si(OH)_4 is
479 not in limiting conditions, i.e. $> 5 \text{ mmol m}^{-3}$.

480 6. Acknowledgement

481 We would like to thank the captain and crew of RV Polarstern and fellow expeditioners
482 for their assistance during the ANT-XVIII/III “Eddy-Pump” cruise. We thank NASA for
483 providing the MODIS Chl-a and PAR data, and the SeaWiFS Chl-a data, and NOAA for
484 the AVHRR data. We also thank ESA for the MERIS Chl-a data and the OC-CCI merged
485 Chl-a data. This work was supported by the HGF Innovative Network Funds (Phytooptics)
486 and DFG in the framework of the priority programme ”Antarctic Research with comparative
487 investigations in Arctic ice areas” by a grant HO 4680/1.

488 7. References

- 489 Alderkamp, A.C., de Baar, H.J.W., Visser, R.J.W., Arrigo, K.R., 2010. Can photoinhibition control phy-
490 toplankton abundance in deeply mixed water columns of the southern ocean? *Limnol. Oceanogr.* 55,
491 1248–1264.
- 492 Alderkamp, A.C., Kulk, G., Buma, A.G.J., Visser, R.J.W., Van Dijken, G.L., Mills, M.M., Arrigo, K.R.,
493 2012. The effect of iron limitation on the photophysiology of *Phaeocystis antarctica* (Prymnesiophyceae)
494 and *Fragilariopsis cylindrus* (Bacillariophyceae) under dynamic irradiance. *J. Phycol.* 48, 45–59. doi:[10.1111/j.1529-8817.2011.01098.x](https://doi.org/10.1111/j.1529-8817.2011.01098.x).
- 495
496 Arrigo, K., Ditullio, G., Dunbar, R., Robinson, D., Vanwoert, M., Worthen, D., Lizotte, M., 2000. Phyto-
497 plankton taxonomic variability in nutrient utilization and primary production in the ross sea. *J. Geophys.*
498 *Res.* 105, 8827–8845. doi:[10.1029/1998JC000289](https://doi.org/10.1029/1998JC000289).

- 499 de Baar, H.J.W., Boyd, P.W., Coale, K.H., Landry, M.R., Tsuda, A., Assmy, P., Bakker, D.C.E., Bozec, Y.,
500 Barber, R.T., Brzezinski, M.A., Buesseler, K.O., Boyè, M., Croot, P.L., Gervais, F., Gorbunov, M.Y.,
501 Harrison, P.J., Hiscock, W.T., Laan, P., Lancelot, C., Law, C.S., Levasseur, M., Marchetti, A., Millero,
502 F.J., Nishioka, J., Nojiri, Y., van Oijen, T., Riebesell, U., Rijkenberg, M.J.A., Saito, H., Takeda, S.,
503 Timmermans, K.R., Veldhuis, M.J.W., Waite, A.M., Wong, C.S., 2005. Synthesis of iron fertilization
504 experiments: From the iron age in the age of enlightenment. *J. Geophys. Res.* 110, C09S16. doi:[10.1029/
505 2004JC002601](https://doi.org/10.1029/2004JC002601).
- 506 Banse, K., 1996. Low seasonality of low concentrations of surface chlorophyll in the subantarctic water
507 ring: underwater irradiance, iron, or grazing? *Progress in Oceanography* 37, 241–291. doi:[10.1016/
508 S0079-6611\(96\)00006-7](https://doi.org/10.1016/S0079-6611(96)00006-7).
- 509 Barlow, R., Cummings, D., Gibb, S., 1997. Improved resolution of mono-and divinyl chlorophylls *a* and *b*
510 and zeaxanthin and lutein in phytoplankton extracts using reverse phase C-8 HPLC. *Mar. Ecol. Prog.*
511 *Ser.* 161, 303–307.
- 512 Bowie, A.R., Griffiths, F.B., Dehairs, F., Trull, T.W., 2011. Oceanography of the subantarctic and Polar
513 Frontal Zones south of Australia during summer: Setting for the SAZ-Sense study. *Deep-Sea Res. II* 58,
514 2059 – 2070. doi:[10.1016/j.dsr2.2011.05.033](https://doi.org/10.1016/j.dsr2.2011.05.033).
- 515 Boyd, P.W., 2002. Environmental factors controlling phytoplankton processes in the Southern Ocean. *J.*
516 *Phycol.* 38, 844–861. doi:[10.1046/j.1529-8817.2002.t01-1-01203.x](https://doi.org/10.1046/j.1529-8817.2002.t01-1-01203.x).
- 517 Boyd, P.W., Jickells, T., Law, C.S., Blain, S., Boyle, E.A., Buesseler, K.O., Coale, K.H., Cullen, J.J.,
518 de Baar, H.J.W., Follows, M., Harvey, M., Lancelot, C., Levasseur, M., Owens, N.P.J., Pollard, R.,
519 Rivkin, R.B., Sarmiento, J., Schoemann, V., Smetacek, V., Takeda, S., Tsuda, A., Turner, S., Watson,
520 A.J., 2007. Mesoscale iron enrichment experiments 1993-2005: Synthesis and future directions. *Science*
521 315, 612–617. doi:[10.1126/science.1131669](https://doi.org/10.1126/science.1131669).
- 522 Brunet, C., Lavaud, J., 2010. Can the xanthophyll cycle help extract the essence of the microalgal functional
523 response to a variable light environment? *J. Plankton Res.* 32, 1609–1617. doi:[10.1093/plankt/fbq104](https://doi.org/10.1093/plankt/fbq104).
- 524 Cheah, W., Mcminn, A., Griffiths, F.B., Westwood, K.J., Wright, S.W., Clementson, L.A., 2013. Response
525 of phytoplankton photophysiology to varying environmental conditions in the Sub-Antarctic and Polar
526 Frontal Zone. *PLoS ONE* 8, e72165. doi:[10.1371/journal.pone.0072165](https://doi.org/10.1371/journal.pone.0072165).
- 527 Clementson, L., Parslow, J., Turnbull, A., McKenzie, D., Rathbone, C., 2001. Optical properties of waters
528 in the Australasian sector of the Southern Ocean. *J. Geophys. Res.* 106, 31611–31625. doi:[10.1029/
529 2000JC000359](https://doi.org/10.1029/2000JC000359).
- 530 Falkowski, P.G., La Roche, J., 1991. Acclimation to spectral irradiance in algae. *J. Phycol.* 27, 8–14.
531 doi:[10.1111/j.0022-3646.1991.00008.x](https://doi.org/10.1111/j.0022-3646.1991.00008.x).
- 532 Franck, V.M., Brzezinski, M.A., Coale, K.H., Nelson, D.M., 2000. Iron and silicic acid concentrations
533 regulate Si uptake north and south of the Polar Frontal Zone in the Pacific Sector of the Southern Ocean.
534 *Deep-Sea Res. II* 47, 3315–3338. doi:[10.1016/S0967-0645\(00\)00070-9](https://doi.org/10.1016/S0967-0645(00)00070-9).
- 535 Goss, R., Jakob, T., 2010. Regulation and function of xanthophyll cycle-dependent photoprotection in algae.
536 *Photosynth. Res.* 106, 103–122. doi:[10.1007/s11120-010-9536-x](https://doi.org/10.1007/s11120-010-9536-x).
- 537 Greene, R.M., Geider, R.J., Kolber, Z., Falkowski, P.G., 1992. Iron-induced changes in light harvesting
538 and photochemical energy conversion processes in eukaryotic marine algae. *Plant Physiol.* 100, 565–575.
539 doi:[10.1104/pp.100.2.565](https://doi.org/10.1104/pp.100.2.565).
- 540 Hauck, J., Völker, C., Wang, T., Hoppema, M., Losch, M., Wolf-Gladrow, D.A., 2013. Seasonally different
541 carbon flux changes in the Southern Ocean in response to the southern annular mode. *Global Biogeochem.*
542 *Cycles* 27, 1236–1245. doi:[10.1002/2013GB004600](https://doi.org/10.1002/2013GB004600).
- 543 Higgins, H.W., Wright, S.W., Schlüter, L., 2011. Quantitative interpretation of chemotaxonomic pigment
544 data, in: Roy, S., Egeland, E.S., Johnsen, G., Llewellyn, C.A. (Eds.), *Phytoplankton pigments: Char-*
545 *acterization, chemotaxonomy and applications in oceanography.* Cambridge University Press. chapter 6,
546 pp. 257–313.
- 547 Hiscock, M., Marra, J., Smith, W., Goericke, R., Measures, C., Vink, S., Olson, R., Sosik, H., Barber, R.,
548 2003. Primary productivity and its regulation in the Pacific Sector of the Southern Ocean. *Deep-Sea Res.*
549 *II* 50, 533–558. doi:[10.1016/S0967-0645\(02\)00583-0](https://doi.org/10.1016/S0967-0645(02)00583-0).

- 550 Hoppe, C.J.M., Klaas, C., Ossebaar, S., Soppa, M.A., Cheah, W., Rost, B., Wolf-Gladrow, D.A., Bracher, A.,
551 Hoppema, M., Strass, V., Trimborn, S., this issue. Controls of primary production in two phytoplankton
552 blooms in the Antarctic Circumpolar Current. Accepted in Deep-Sea Res. II .
- 553 Hutchins, D.A., Sedwick, P.N., DiTullio, G.R., Boyd, P.W., Queguiner, B., Griffiths, F.B., Crossley, C.,
554 2001. Control of phytoplankton growth by iron and silicic acid availability in the subantarctic Southern
555 Ocean: Experimental results from the SAZ Project. *J. Geophys. Res.* 106, 31559–31572. doi:[10.1029/
556 2000JC000333](https://doi.org/10.1029/2000JC000333).
- 557 Khatiwala, S., Primeau, F., Hall, T., 2009. Reconstruction of the history of anthropogenic CO₂ concentra-
558 tions in the ocean. *Nature* 462, 346–349. doi:[10.1038/nature08526](https://doi.org/10.1038/nature08526).
- 559 Khatiwala, S., Tanhua, T., Mikaloff Fletcher, S., Gerber, M., Doney, S.C., Graven, H.D., Gruber, N.,
560 McKinley, G.A., Murata, A., Ríos, A.F., Sabine, C.L., 2013. Global ocean storage of anthropogenic
561 carbon. *Biogeosciences* 10, 2169–2191. doi:[10.5194/bg-10-2169-2013](https://doi.org/10.5194/bg-10-2169-2013).
- 562 Kolber, Z., Falkowski, P.G., 1993. Use of active fluorescence to estimate phytoplankton photosynthesis in
563 situ. *Limnol. Oceanogr.* 38, 1646–1665.
- 564 Kolber, Z.S., Barber, R.T., Coale, K.H., Fitzwater, S.E., Greene, R.M., Johnson, K.S., Lindley, S.,
565 Falkowski, P.G., 1994. Iron limitation of phytoplankton photosynthesis in the equatorial Pacific Ocean.
566 *Nature* 371, 145–149. doi:[10.1038/371145a0](https://doi.org/10.1038/371145a0).
- 567 Kolber, Z.S., Prasil, O., Falkowski, P.G., 1998. Measurements of variable chlorophyll fluorescence using fast
568 repetition rate techniques: defining methodology and experimental protocols. *Biochim. Biophys. Acta*
569 1367, 88–106. doi:[10.1016/S0005-2728\(98\)00135-2](https://doi.org/10.1016/S0005-2728(98)00135-2).
- 570 Kropuenske, L.R., Mills, M.M., van Dijken, G.L., Alderkamp, A.C., Berg, G.M., Robinson, D.H.,
571 Welschmeyer, N.A., Arrigo, K.R., 2010. Strategies and rates of photoacclimation in two major Southern
572 Ocean phytoplankton taxa: *Phaeocystis antarctica* (Haptophyta) and *Fragilariopsis cylindrus* (Bacillar-
573 iophyceae). *J. Phycol.* 46, 1138–1151. doi:[10.1111/j.1529-8817.2010.00922.x](https://doi.org/10.1111/j.1529-8817.2010.00922.x).
- 574 Laglera, L.M., Santos-Echeandía, J., Caprara, S., Monticelli, D., 2013. Quantification of iron in seawater
575 at the low picomolar range based on optimization of bromate/ammonia/dihydroxynaphtalene system by
576 catalytic adsorptive cathodic stripping voltammetry. *Analytical Chemistry* 85, 2486–2492. doi:[10.1021/
577 ac303621q](https://doi.org/10.1021/ac303621q).
- 578 Landschützer, P., Gruber, N., Haumann, F.A., Rödenbeck, C., Bakker, D.C.E., van Heuven, S., Hoppema,
579 M., Metzl, N., Sweeney, C., Takahashi, T., Tilbrook, B., Wanninkhof, R., 2015. The reinvigoration of the
580 Southern Ocean carbon sink. *Science* 349, 1221–1224. doi:[10.1126/science.aab2620](https://doi.org/10.1126/science.aab2620).
- 581 Louda, J.W., Li, J., Liu, L., Winfree, M.N., Baker, E.W., 1998. Chlorophyll-a degradation during cellular
582 senescence and death. *Organic Geochemistry* 29, 1233–1251. doi:[10.1016/S0146-6380\(98\)00186-7](https://doi.org/10.1016/S0146-6380(98)00186-7).
- 583 Mackey, M.D., Mackey, D.J., Higgins, H.W., Wright, S.W., 1996. CHEMTAX - a program for estimating
584 class abundances from chemical markers: application to HPLC measurements of phytoplankton. *Mar.*
585 *Ecol. Prog. Ser.* 144, 265–283. doi:[10.3354/meps144265](https://doi.org/10.3354/meps144265).
- 586 McKew, B.A., Davey, P., Finch, S.J., Hopkins, J., Lefebvre, S.C., Metodiev, M.V., Oxborough, K., Raines,
587 C.A., Lawson, T., Geider, R.J., 2013. The trade-off between the light-harvesting and photoprotective
588 functions of fucoxanthin-chlorophyll proteins dominates light acclimation in *Emiliania huxleyi* (clone
589 CCMP 1516). *New Phytol.* 200, 74–85. doi:[10.1111/nph.12373](https://doi.org/10.1111/nph.12373).
- 590 Moore, C.M., Seeyave, S., Hickman, A.E., Allen, J.T., Lucas, M.I., Planquette, H., Pollard, R.T., Poul-
591 ton, A.J., 2007. Iron-light interactions during the CROZet natural iron bloom and EXport exper-
592 iment (CROZEX) I: Phytoplankton growth and photophysiology. *Deep-Sea Res. II* 54, 2045–2065.
593 doi:[10.1016/j.dsr2.2007.06.011](https://doi.org/10.1016/j.dsr2.2007.06.011).
- 594 Moore, C.M., Suggett, D.J., Hickman, A.E., Kim, Y.N., Tweddle, J.F., Sharples, J., Geider, R.J., Holligan,
595 P.M., 2006. Phytoplankton photoacclimation and photoadaptation in response to environmental gradients
596 in a shelf sea. *Limnol. Oceanogr.* 51, 936–949. doi:[10.4319/lo.2006.51.2.0936](https://doi.org/10.4319/lo.2006.51.2.0936).
- 597 Morel, A., Maritorena, S., 2001. Bio-optical properties of oceanic waters: A reappraisal. *J. Geophys. Res.*
598 106, 7163–7180. doi:[10.1029/2000JC000319](https://doi.org/10.1029/2000JC000319).
- 599 Morrison, A.K., Frölicher, T.L., Sarmiento, J.L., 2015. Upwelling in the Southern Ocean. *Physics Today* ,
600 27–32.

601 OC-CCI, 2015. Ocean Colour Climate Change Initiative (OC-CCI) – Phase Two - Product User Guide.
602 2.0.5 ed. Plymouth Marine Laboratory.

603 Olaizola, M., Roche, J., Kolber, Z., Falkowski, P.G., 1994. Non-photochemical fluorescence quenching and
604 the diadinoxanthin cycle in a marine diatom. *Photosynth. Res.* 41, 357–370. doi:[10.1007/BF00019413](https://doi.org/10.1007/BF00019413).

605 Pearce, I., Davidson, A.T., Thomson, P.G., Wright, S., van den Enden, R., 2011. Marine microbial ecology
606 in the sub-Antarctic Zone: Rates of bacterial and phytoplankton growth and grazing by heterotrophic
607 protists. *Deep-Sea Res. II* 58, 2248–2259. doi:[10.1016/j.dsr2.2011.05.030](https://doi.org/10.1016/j.dsr2.2011.05.030).

608 van de Poll, W.H., Janknegt, P.J., van Leeuwe, M.A., Visser, R.J.W., Buma, A.G.J., 2009. Excessive
609 irradiance and antioxidant responses of an antarctic marine diatom exposed to iron limitation and to
610 dynamic irradiance. *J. Photoch. Photobiol. B* 94, 32–37. doi:[10.1016/j.jphotobiol.2008.09.003](https://doi.org/10.1016/j.jphotobiol.2008.09.003).

611 van de Poll, W.H., Visser, R.J.W., Buma, A.G.J., 2007. Acclimation to a dynamic irradiance regime changes
612 excessive irradiance sensitivity of *Emiliania huxleyi* and *Thalassiosira weissflogii*. *Limnol. Oceanogr.* 52,
613 1430–1438. doi:[10.4319/lo.2007.52.4.1430](https://doi.org/10.4319/lo.2007.52.4.1430).

614 Puigcorb , V., Roca-Mart , M., Masqu , P., Benitez-Nelson, C., van der Loeff, M.R., Laglera, L.M., Bracher,
615 A., Cheah, W., Strass, V., Hoppema, M., Santos-Echeand a, J., Klaas, C., this issue. Particulate organic
616 carbon export across the Antarctic Circumpolar Current at 10 E: Differences north and south of the
617 Antarctic Polar Front. Submitted to *Deep-Sea Res. II* .

618 R Core Team, 2014. R: A Language and Environment for Statistical Computing. R Foundation for Statistical
619 Computing. Vienna, Austria.

620 Rintoul, S.R., Trull, T.W., 2001. Seasonal evolution of the mixed layer in the Subantarctic Zone south of
621 Australia. *J. Geophys. Res.* 106, 31447–31462. doi:[10.1029/2000jc000329](https://doi.org/10.1029/2000jc000329).

622 Sabine, C.L., Feely, R.A., Gruber, N., Key, R.M., Lee, K., Bullister, J.L., Wanninkhof, R., Wong, C.S.,
623 Wallace, D.W.R., Tilbrook, B., Millero, F.J., Peng, T.H., Kozyr, A., Ono, T., Rios, A.F., 2004. The
624 Oceanic Sink for Anthropogenic CO₂. *Science* 305, 367–371. doi:[10.1126/science.1097403](https://doi.org/10.1126/science.1097403).

625 de Salas, M.F., Eriksen, R., Davidson, A.T., Wright, S.W., 2011. Protistan communities in the Australian
626 sector of the Sub-Antarctic Zone during SAZ-Sense. *Deep-Sea Res. II* 58, 2135 – 2149. doi:[10.1016/j.dsr2.2011.05.032](https://doi.org/10.1016/j.dsr2.2011.05.032).

627 Smith, R.C., Booth, C.R., Star, J.L., 1984. Oceanographic biooptical profiling system. *Applied Optics* 23,
628 2791–2797. doi:[10.1364/AO.23.002791](https://doi.org/10.1364/AO.23.002791).

629 Soppa, M., Dinter, T., Taylor, B., Bracher, A., 2013. Satellite derived euphotic depth in the Southern
630 Ocean: Implications for primary production modelling. *Remote Sensing of Environment* 137, 198 – 211.
631 doi:[10.1016/j.rse.2013.06.017](https://doi.org/10.1016/j.rse.2013.06.017).

632 Soppa, M.A., Hirata, T., Silva, B., Dinter, T., Peeken, I., Wiegmann, S., Bracher, A., 2014. Global retrieval
633 of diatom abundance based on phytoplankton pigments and satellite data. *Remote Sensing* 6, 10089–
634 10106. URL: , doi:[10.3390/rs61010089](https://doi.org/10.3390/rs61010089).

635 Stramski, D., Reynolds, R.A., Babin, M., Kaczmarek, S., Lewis, M.R., R ttgers, R., Sciandra, A., Stramska,
636 M., Twardowski, M.S., Franz, B.A., Claustre, H., 2008. Relationships between the surface concentration
637 of particulate organic carbon and optical properties in the eastern South Pacific and eastern Atlantic
638 Oceans. *Biogeosciences* 5, 171–201. doi:[10.5194/bg-5-171-2008](https://doi.org/10.5194/bg-5-171-2008).

639 Strass, V., 1990. On the calibration of large-scale fluorometric chlorophyll measurements from towed undu-
640 lating vehicles. *Deep-Sea Res. Part A.* 37, 525–540. doi:[10.1016/0198-0149\(90\)90023-0](https://doi.org/10.1016/0198-0149(90)90023-0).

641 Strass, V., Leach, H., Prandke, H., Donnelly, M., Bracher, A., Wolf-Gladrow, D., this issue. The physical
642 environmental conditions for biogeochemical differences along the Antarctic Circumpolar Current in the
643 Atlantic Sector during late austral summer 2012. Submitted to *Deep-Sea Res. II* .

644 Strzpeke, R.F., Harrison, P.J., 2004. Photosynthetic architecture differs in coastal and oceanic diatoms.
645 *Nature* 431, 689–92. doi:[10.1038/nature02954](https://doi.org/10.1038/nature02954).

646 Suggett, D.J., Moore, C.M., Hickman, A.E., Geider, R.G., 2009. Interpretation of fast repetition rate
647 (FRR) fluorescence: signatures of phytoplankton community structure versus physiological state. *Mar.*
648 *Ecol. Prog. Ser.* 376, 1 – 9. doi:[10.3354/meps07830](https://doi.org/10.3354/meps07830).

649 Suggett, D.J., Moore, C.M., Mara n n, E., Omachi, C., Varela, R.A., Aiken, J., Holligan, P.M., 2006.
650 Photosynthetic electron turnover in the tropical and subtropical Atlantic Ocean. *Deep-Sea Res. II* 53,
651

- 652 1573–1592. doi:[10.1016/j.dsr2.2006.05.014](https://doi.org/10.1016/j.dsr2.2006.05.014).
- 653 Sunda, W.G., Huntsman, S.A., 1997. Interrelated influence of iron, light and cell size on marine phytoplank-
654 ton growth. *Nature* 390, 389–392. doi:[10.1038/37093](https://doi.org/10.1038/37093).
- 655 Taylor, B.B., Torrecilla, E., Bernhardt, A., Taylor, M.H., Peeken, I., Röttgers, R., Piera, J., Bracher, A.,
656 2011. Bio-optical provinces in the eastern Atlantic Ocean and their biogeographical relevance. *Biogeo-*
657 *sciences* 8, 3609–3629. doi:[10.5194/bg-8-3609-2011](https://doi.org/10.5194/bg-8-3609-2011).
- 658 Uitz, J., Claustre, H., Griffiths, F.B., Ras, J., Garcia, N., Sandronie, V., 2009. A phytoplankton class-specific
659 primary production model applied to the Kerguelen Islands region (Southern Ocean). *Deep-Sea Res. I*
660 56, 541–560. doi:[10.1016/j.dsr.2008.11.006](https://doi.org/10.1016/j.dsr.2008.11.006).
- 661 Uitz, J., Huot, Y., Bruyant, F., Babin, M., Claustre, H., 2008. Relating phytoplankton photophysiological
662 properties to community structure on large scales. *Limnol. Oceanogr.* 53, 614–630. doi:[10.4319/lo.](https://doi.org/10.4319/lo.2008.53.2.0614)
663 [2008.53.2.0614](https://doi.org/10.4319/lo.2008.53.2.0614).
- 664 Westwood, K.J., Griffiths, F.B., Webb, J.P., Wright, S.W., 2011. Primary production in the Sub-Antarctic
665 and Polar Frontal Zones south of Tasmania, Australia; SAZ-Sense survey, 2007. *Deep-Sea Res. II* 58,
666 2162 – 2178. doi:[10.1016/j.dsr2.2011.05.017](https://doi.org/10.1016/j.dsr2.2011.05.017).
- 667 Wright, S.W., van den Enden, R.L., Pearce, I., Davidson, A.T., Scott, F.J., Westwood, K.J., 2010. Phyto-
668 plankton community structure and stocks in the Southern Ocean (30-80°E) determined by CHEMTAX
669 analysis of HPLC pigment signatures. *Deep-Sea Res. II* 57, 758–778. doi:[10.1016/j.dsr2.2009.06.015](https://doi.org/10.1016/j.dsr2.2009.06.015).